

The Mass-Temperature Relation for B and Early A Stars Based on *IUE* Spectra of Detached Eclipsing Binaries

NANCY REMAGE EVANS,¹ MCKENZIE G. FERRARI,² JOANNA KURASZKIEWICZ,¹ STEVEN SILVERBERG,¹ JOY NICHOLS,¹
GUILLERMO TORRES,¹ AND MAKENZI FISCHBACH³

¹*Center for Astrophysics | Harvard & Smithsonian
60 Garden St.*

Cambridge, MA 02138, USA

²*University of Massachusetts-Dartmouth
285 Old Westport Rd.*

North Dartmouth, MA 02747

³*Wellesley College
Wellesley, MA*

ABSTRACT

Ultraviolet spectra were taken of 25 Detached Eclipsing Binaries (DEBs) with spectral types O, B, and early A with the *International Ultraviolet Explorer (IUE)* satellite in the 1150 to 1900 Å region. The spectra were compared with BOSZ model atmospheres (Bohlin, et al. 2017). The composite spectra of the DEBs were modeled by a combination of models representing the hot and cool components, and the temperatures of the hottest components of the systems were determined. From these temperatures a direct Mass-Temperature relation was obtained for stars close to the main sequence with solar metallicity for B and early A stars:

$$\log M_{\odot} = -5.90 \pm 0.27 + (1.56 \pm 0.07) \times \log T$$

This relation allows a mass to be inferred for comparable stars from an ultraviolet spectrum. The five chemically peculiar Am stars in the sample have larger radii than normal A stars of the same mass.

Keywords: early-type stars — ultraviolet spectroscopy — eclipsing binary stars — effective temperature

1. INTRODUCTION

Observationally measured masses are critical to understanding stars. Evolution calculations are tied to these measures. Eclipsing binary systems where the inclination of the system can be determined are a crucial part of the sample of stars for which we have accurate masses. Andersen (1991) compiled a list of detached eclipsing binaries (DEBs) with accurately determined masses. This list has subsequently been updated by Torres, Andersen, and Gimenez (2010; TAG below).

Well covered photometric and spectroscopic curves analyzed with modern software provide highly accurate masses, radii, and temperature ratios between the two components of the system. However a valuable parameter in relating these properties to, for example, evolutionary tracks is the temperature of each of the two

stars. These must be determined from, for instance, spectral types.

When the Andersen list was drawn up, the *International Ultraviolet Explorer (IUE)* Satellite was operating. It provided well calibrated spectra particularly in the 1150 to 1900 Å ultraviolet (UV) region. For stars of A spectral types and hotter, a large fraction of the flux is contained in this spectral region. For this reason a program was set up to observe eclipsing systems from the Andersen list with primaries in this spectral type range. Comparison of these spectra with atmospheric models provides a temperature for the primary. The goal of this study is to obtain a temperature which describes the energy distribution in this important wavelength region. This results in a *direct* mass-temperature relation for hot stars, which can be used to infer the mass of a star from ultraviolet spectra.

2. OBSERVATIONS

The *International Ultraviolet Explorer (IUE)* Satellite was launched in 1978 and was operated by NASA, ESA

and the British SERC. It provided spectra in the wavelength regions 1150 to 1975 Å and 1910 to 3300 Å, in two resolution modes (resolution 0.1 and 6 Å respectively for high and low resolution). Full details of the satellite, spectrographs and cameras are given in Harris and Sonneborn (1987).

For eclipsing binaries which have an O, B, or early A component we obtained low resolution spectra with the IUE satellite in the short wavelength region through the large aperture. These were largely from the program TEPNE (PI: Evans), supplemented by archival data when available. The observations are summarized in Table 1. Columns list the variable star designation, the HD or BD number, the exposure time, the spectrum number, the observing date and the observing time, the maximum data count (Data Numbers) in the spectrum and the background count. Most spectra were well exposed; however a maximum count of 255 means some part of the spectrum is saturated and cannot be used.

Table 2 provides the orbital phases at which the *IUE* observations were obtained. Columns list the system, the period, the HJD of primary minimum, the reference for the orbit, the phase of secondary minimum, the HJD of the *IUE* observation, the orbital phase of the *IUE* observation, and notes. Most of the *IUE* observations were taken outside of eclipse. In the final column asterisks indicate 4 systems for which the observation occurred during some part of an eclipse. Three of these systems (V478 Cyg, AH Cep, and V587 Mon) were discarded during spectral fitting, as discussed in Section 5. V539 Ara was also mildly affected by an eclipse, as is also discussed in Section 5.

3. DATA REDUCTION

Spectra were retrieved from the Hubble Space Telescope (HST) Mikulski Archive for Space Telescope (MAST) archive, having been processed with the NEWSIPS pipeline (Nichols and Linsky 1996). Further processing was done with the IUE Regional Analysis Facility (IUERDAF) software package installed at the Harvard & Smithsonian Center for Astrophysics, High Energy Division. The correction to the IUE fluxes derived by Bohlin and Bianchi (2017) to match the HST CALSPEC files (e.g. Space Telescope Imaging Spectrograph [STIS] spectra) was applied to the IUE fluxes.

IUE NEWSIPS pipeline already removes known features such as the reseaux marks on the camera and cosmic ray hits. In addition, for most exposure times geocoronal Lyman α emission is present in the line cores, which was removed (“blemished”) by eye. The spectra were then dereddened using the reddening law of Cardelli, Clayton, and Mathis (1989) using the IDL pro-

cedure `unred_ccm.pro`. $E(B-V)$ was taken from TAG (except for WX Cep) and is listed in the summary table (Table 6). The reddening for WX Cep was taken from Graczyk, et al. (2019).

3.1. BOSZ Model Atmospheres

A grid of stellar atmospheres has been computed by Bohlin et al. (2017) from the Kurucz Atlas9 code, which are available in the MAST archive.

To cover a range of hot stars, we used an initial 58 models spanning a temperature range of 5,000–35,000 K. For the BOSZ models used in this work, we chose the following initial conditions appropriate to main sequence stars in *IUE* low resolution spectra: surface gravity ($\log g$) = 4.0, solar metallicity $[M/H] = 0$, solar carbon abundance $[C/M] = \text{solar}$, alpha abundance $[\alpha/M] = 0$, instrumental broadening = 500 km/s, and microturbulence = 2 km/s. The selection of these parameters was to reflect the characteristics of the DEBs and *IUE* spectra as closely as possible, while keeping the analysis uniform for all systems.

While the BOSZ temperature models span a large temperature range, the increments at which a temperature model is available varies throughout the range. For cooler temperatures, models are available every 250 K. For warmer temperatures, models are available every 500 K. At the hottest temperatures, models are available every 1000 K. To determine more precise temperature uncertainties, we generated linearly interpolated models from the original BOSZ models.

4. ANALYSIS

The goal of this study was to determine a temperature which best reproduced the spectrum from 1150 to 1975 Å within the framework of the models. The most important aspects of the analysis approach are:

- The composite spectrum of the binary was modeled with a combination of spectra from the models of the hot and cool components.
- The hotter star in the binary dominates at the shortest wavelengths, and only that temperature is determined from the fits.
- The analysis is based on best-determined parameters from the eclipse solution: the mass M , the radius R , and the ratio of temperatures of the two stars T_1/T_2 where 1 and 2 refer to the primary (most massive) and secondary of the binary system.

The details of the matching process are described in the sections below.

4.1. Spectrum–Model Comparisons

The comparison between the IUE spectrum and the BOSZ models was made as follows. The radii of the

Table 1. *IUE* Satellite Spectra for DEBs

System	ID	Exposure (s)	Spectrum ID	Obs Date	Obs Time	Max Count	Background
V478 Cyg	HD 193611	427.5	SWP48207	1993/07/22	16:50:08	72	16
AH Cep	HD 216014	89.6	SWP10148	1980/09/16	5:07:28	255	17
V578 Mon	HD 259135	2699.5	SWP17905	1982/09/10	9:21:56	178	58
QX Car	HD 86118	4.8	SWP50174	1994/03/06	22:20:14	179	14
V539 Ara	HD 161783	2.7	SWP48476	1993/08/27	16:25:07	132	16
CV Vel	HD 77464	4.4	SWP50160	1994/03/03	20:46:04	118	16
U Oph	HD 156247	10.5	SWP48498	1993/08/29	15:14:27	189	15
V760 Sco	HD 147683	41.6	SWP48497	1993/08/29	14:10:13	138	15
GG Lup	HD 135876	8.5	SWP48496	1993/08/29	12:58:18	255	17
ζ Phe	HD 6882	1.1	SWP48495	1993/08/29	11:37:37	143	16
χ² Hya	HD 96314	6.8	SWP50685	1994/05/03	20:28:43	108	15
IQ Per	HD 24909	111.7	SWP50177	1994/03/07	2:19:11	192	16
PV Cas	HD 240208	880.5	SWP48206	1993/07/22	15:43:50	99	19
V451 Oph	HD 170470	208.8	SWP48217	1993/07/23	18:52:14	181	16
WX Cep	HD 213631	2999.1	SWP50179	1994/03/07	20:38:38	109	19
TZ Men	HD 39780	29.8	SWP50175	1994/03/06	23:26:55	164	15
V1031 Ori	HD 38735	69.5	SWP50176	1994/03/07	0:39:52	132	15
β Aur	HD 40183	0.7	SWP50172	1994/03/06	19:34:58	114	14
YZ Cas	HD 4161	39.6	SWP26934	1985/10/14	14:00:51	183	18
V624 Her	HD 161321	85.5	SWP48216	1993/07/23	17:35:04	104	16
GZ CMa	HD 56429	419.7	SWP50173	1994/03/06	20:55:47	126	16
V1647 Sgr	HD 163708	99.8	SWP48475	1993/08/27	15:35:53	150	15
EE Peg	HD 206155	119.5	SWP50684	1994/05/03	19:04:41	139	17
VV Pyx	HD 71581	77.7	SWP50161	1994/03/03	22:08:02	189	15
AY Cam	BD+77° 328	2699.5	SWP29742	1986/11/24	1:41:45	63	21

primary and secondary stars in the systems are well determined from the eclipse solutions. The analysis was started with the temperatures T_1 and T_2 from spectral types from TAG. A model atmosphere was selected close to the temperature for each star, and then the model of the secondary was scaled using $(R_2/R_1)^2$ from the eclipse solutions. These two models were then summed and normalized to the flux of the *IUE* spectrum. For the hottest stars, the Ly α region (1180 to 1250 Å) was excluded because of contamination by interstellar Ly α absorption. The summed model flux and the *IUE* flux were then used to calculate a standard deviation (SD). The hottest star (generally the primary) dominates heavily at the shortest wavelengths, so a series of comparisons were made stepping the temperature of the primary T_1 through a series of temperatures bracketing the temperature expected from TAG. These comparisons were used in two ways. First, the comparison was inspected as in Fig. 1. In general, this inspection showed differences between models of T_1 of 100 to 200 K for the cooler primaries and 500 K for hotter primaries. Second the difference between the composite model and the *IUE* spectrum was formed and plotted through the sequence of T_1 (Fig. 2). Again, in general, differences were clear between temperatures (T_1) of about 200 K, particularly at the long and short wavelength regions of the spectra.

The standard deviations produced a parabola as a function of T_1 (Fig. 3), from which the minimum was used to determine T_1 .

Visual inspection of the spectral comparison and the difference plots was one approach to temperature determination. In this case, an uncertainty was estimated from the temperatures which could be identified by eye as too high and too low to be matches (δT_1). The temperature was assumed to be between these temperatures, or a quarter of δT_1 .

We also tried a χ^2 approach, using the *IUE* instrumental error. However, because the study covered a large range of temperatures from 30,000 to 7,000 K two effects complicated the χ^2 estimation. First, different wavelength regions were very differently exposed on the camera, and hence had very different distributions of actual uncertainties. Second the line opacity is very different over that temperature range. Both these were difficult to incorporate into the analysis. Standard deviations seemed to give more consistent temperature uncertainties throughout the range.

Spectral comparisons such as Fig. 1 show the full spectrum. However, portions of the spectrum which are saturated are marked in the upper left spectrum, as are reseau marks, and geocoronal Ly α . While these regions are shown in the figure, they are omitted from the

Table 2. *Phases of Observation*

System	P	Min I	Ref	Phase of Min II	<i>IUE</i>	<i>IUE</i> Phase	Notes
	(d)	HJD			HJD		
V478 Cyg	2.88090063	2444777.4852	1	0.5067	2449191.2014	0.0613	*
AH Cep	1.774761	2445962.7359	2	0.5000	2444498.7135	0.0876	*
V578 Mon	2.40848	2449360.625	3	0.4507	2445222.8902	0.0141	*
QX Car	4.4780399	2443343.41512	4	0.4010	2449418.4307	0.6238	
V539 Ara	3.169112	2445056.777	5	0.3307	2449227.1841	0.9545	*
CV Vel	6.889494	2442048.66894	6	0.5000	2449415.3653	0.2652	
U Oph	1.6773458	2442621.6212	7	0.5017	2449229.1350	0.2675	
V760 Sco	1.7309295	2443250.8268	8	0.5101	2449229.0904	0.7881	
GG Lup	1.84960	2446136.7398	9	0.5064	2449229.0404	0.8754	
ζ Phe	1.6697724	2441643.6890	10	0.5000	2449228.9844	0.7122	
χ ² Hya	2.267701	2442848.6107	11	0.5000	2449476.3532	0.6704	
IQ Per	1.74356214	2444290.3664	12	0.5222	2449418.5966	0.2374	
PV Cas	1.75047	2449210.7956	13	0.5027	2449191.1554	0.7801	
V451 Oph	2.19659557	2445886.53335	14	0.4978	2449192.2862	0.9438	
WX Cep	3.3784535	2425088.537	15	0.5000	2449419.3601	0.7635	
TZ Men	8.56900	2442403.7085	16	0.5096	2449418.4770	0.6216	
V1031 Ori	3.405565	2444643.665	17	0.5000	2449418.5276	0.0765	
β Aur	3.96004673	2452827.195693	18	0.5000	2449418.3159	0.1819	
YZ Cas	4.46722236	2445583.78664	19	0.5000	2446353.0839	0.2093	
V624 Her	3.894977	2440321.005	20	0.5000	2449192.2326	0.6072	
GZ CMa	4.8008500	2443581.56132	21	0.5000	2449418.3720	0.7869	
V1647 Sgr	3.28279251	2441829.69510	22	0.2621	2449227.1499	0.4031	
EE Peg	2.62821423	2440286.4349	23	0.5000	2449476.2949	0.6176	
VV Pyx	4.5961832	2444620.65895	24	0.4804	2449415.4222	0.2054	
AY Cam	2.73496794	2443572.74441	25	0.5000	2446758.5706	0.8496	

NOTE—*Starred systems are where *IUE* observations overlap eclipse; References: 1. Wolf et al. 2006; 2. Holmgren et al. 1990; 3. Hensberge et al. 2000; 4. Andersen et al. 1983; 5. Clausen 1996; 6. Yakut et al. 2007; 7. Vaz et al. 2007; 8. Andersen et al. 1985; 9. Andersen et al. 1993; 10. Andersen et al. 1983; 11. Clausen and Nordstrom 1978; 12. Wolf et al. 2006; 13. Barenbaum & Etzel 1995; 14. Clausen et al. 1986; 15. Popper 1987; 16. Andersen et al. 1987; 17. Andersen et al. 1990; 18. Southworth et al. 2007; 19. Pavlovski et al. 2014; 20. Popper 1984; 21. Popper et al. 1985; 22. Andersen & Gimenez 1985; 23. Lacy & Popper 1984; 24. Andersen et al. 1984; 25. Williamon et al. 2004

SD calculation. In addition in cool spectra, there are features in the models near 1550Å, and 1700Å. While these appear in the models which have complex opacity, they are not seen in any of the spectra, so they are omitted from the fitting (Fig. 4).

4.2. Composite Spectra: Groups

The detailed analysis was done in four groups.

- Group I: The primary and secondary have fairly similar temperatures
- Group II: The secondary is markedly cooler than the primary
- Group III: The secondary is actually hotter than the primary, i.e. the primary has evolved off the main sequence
- Group IV: What is it?

Group II: These are the easiest to analyze. Because the secondary is significantly cooler than the primary, once the model flux is scaled $(R_2/R_1)^2$, the contribution of the secondary is very small. This means that a modest change in temperature T_2 will have an insignificant effect on the summed model spectrum. Hence the procedure stepping through T_1 values will produce an optimal value of T_1 .

Group I: The analysis is a little more complicated. It begins as for Group II to determine a T_1 using an assumed T_2 . (Solutions for which T_2 was larger than T_1 were discarded.) An additional constraint was then imposed. Since the temperature ratio T_1/T_2 is well determined from the eclipse solution, it can be used to obtain T_2 from the value of T_1 determined in the first step. With this new value of T_2 the process is repeated until a solution converges near the T_1/T_2 from the eclipse solution. Occasionally, the temperatures of the two components are determined to be indistinguishable.

Group III: This group similarly requires iteration, although in this case the ratio of the radii brings the models of the two temperatures closer together, complicating the determination of the temperature of the hotter star.

Group IV: This group contains puzzling or otherwise poorly defined solutions.

4.3. Examples

The analysis process is illustrated with examples from a hot star in the sample V451 Oph, and a cool star YZ Cas, both in Group II.

V451 Oph The spectrum/model comparison, the difference comparison, and standard deviation parabola are shown in Figs. 1, 2, and 3 respectively. In Fig 2 since the temperatures for the primary 11500 and 12500 K are clearly ruled out, an estimate of the “visual” uncertainty for T_1 is 250 K.

YZ Cas As an example of a cooler star YZ Cas is used. The spectrum/model comparison, the difference comparison, and the standard deviation parabola are shown in Figs. 4, 5 and 6. From Fig. 5, the temperatures 8750 and 9250 K are ruled out, making an estimate on the visual uncertainty of 125 K for T_1 . The temperature determination from the SD parabola is shown in Fig. 6

4.4. Sources With One-Temperature Fits

For PV Cas, the temperatures, masses, and radii of both the primary and secondary are assumed to be the same (TAG). In this case, only one temperature T_1 was fit to the model. A 1T fit was also explored in other cases, specifically for CV Vel, QX Car, and VV Pyx.

4.5. Reddening Tests

One of the first concerns in working with stellar energy distributions (SEDs) in the ultraviolet is the effect of reddening on derived temperatures. While the ultraviolet fluxes are heavily affected by reddening or uncertainty in reddening, temperatures derived from ultraviolet SEDs are surprisingly robust to changes in reddening, at least for the temperatures of the stars that we are working with. This is for two reasons. First the wavelength range we are working with is only 750 Å (1150 to 1900 Å), making the variation of flux with a change in $E(B-V)$ within that wavelength range quite small. Second, the observed energy distributions have a well defined shape in flux versus wavelength so that the comparison with the models is fairly tightly defined. For example, the hottest stars typically have flux which decreases sharply at shorter wavelengths.

We have tested the sensitivity of our temperature fits to reddening on a range of $E(B-V)$ values for V451 Oph

Table 3. $E(B-V)$ Tests for V451 Oph

$E(B-V)$	T	\pm
(mag)	(K)	(K)
0.05	11734.9	125
0.10	11933.4	125
0.158	12161.8	250
0.20	12376.3	312
0.25	12639.4	280

(Table 3). The uncertainties in Table 3 are from the visual estimates as discussed in Sect. 4.1. Although the range in $E(B-V)$ is much larger than possible uncertainties in $E(B-V)$, the resulting temperatures only differ by ± 450 K or $\pm 4\%$. Thus for a typical uncertainty in $E(B-V)$ (perhaps 0.03 mag) the uncertainty in the temperature is $<1\%$. In addition, most values of $E(B-V)$ for the targets are very small (Table 6), implying small uncertainties in the reddening and temperature.

4.6. M-K Standards

In order to explore the sensitivity of the fits to IUE spectra of early B stars, three spectra from the IUE Ultraviolet Spectral Atlas (Wu, et al. 1983) of Morgan-Keenan spectral type standards (or similar substitutes where necessary) were analyzed in the same way as the DEBs. Results are provided in Appendix A. For comparison temperatures for several calibrations of the MK classes are provided.

4.7. Temperature Summary

The temperature results are summarized by Group in Table 4. The columns list the star and T_1 from the parabola fit. The two error estimates are from the standard deviation parabola and the visual inspection of the spectrum/model comparison. T_2 is the temperature of the secondary in the fit, starting from the value in TAG, but adjusted if required by the comparisons. The T_2/T_1 ratio from TAG is in the next column. In borderline cases there is a little overlap in this ratio between Group I and Group II. The final column provides notes to our fits. For PV Cas a one-temperature fit was made (Sect. 4.4). For Group III (bottom) T_2 is the hotter temperature and is listed in Column 2 rather than Column 5.

One of the goals of this study was to determine the temperature range for which IUE spectra provide accurate temperatures. This is discussed further in Section 6.

5. COMMENTS ON INDIVIDUAL SYSTEMS

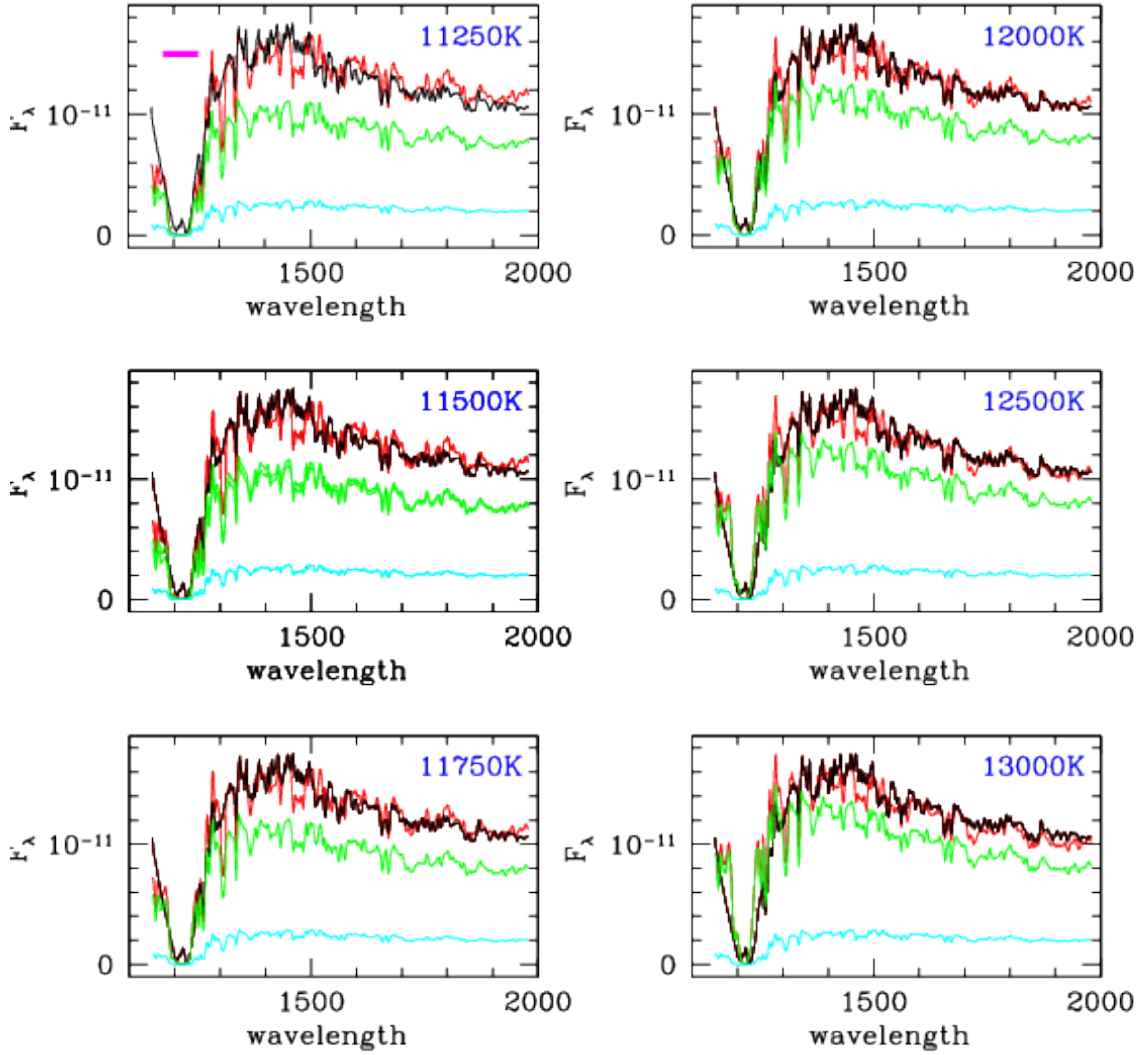


Figure 1. V451 Oph: Comparison of the *IUE* unreddened spectrum and models. Lines are: *IUE* spectrum: black; hot model: green; cool spectrum: blue; model composite: red. Model T_1 (hot) temperatures are indicated in each panel. The best fit is for $T_1 = 12000$ K. Wavelength is in \AA ; flux is in $\text{ergs cm}^{-2} \text{s}^{-1} \text{\AA}^{-1}$ in all figures.

Table 4. Temperatures by Group

Star	T ₁	Err	Err	T ₂	T ₂ /T ₁ ^a	Notes ^b
		SD	Vis			
	(K)	(K)	(K)	(K)		
Group II						
V539 Ara	19248	363	500	17500	0.945	
GG Lup	15793	1518	250	11500	0.746	
ζ Phe	14483	2440	250	12000	0.833	
IQ Per	13241	3051	250	8750	0.626	
TZ Men	10418	1123	100	7250	0.692	
V451 Oph	11980	130	250	11000	0.907	
YZ Cas	8982	385	125	7250	0.706	
V624 Her	8160	335	125	8000	0.975	
GZ CMa	8566	440	125	8250	0.966	
EE Peg	8687	119	125	6500	0.741	
Group I						
QX Car	23428	—	1000	23000	0.950	
CV Vel	18045	563	500	18000	0.989	
V760 Sco	17092	854	500	16000	0.964	
PV Cas	10632	677	250		0.999	1T
β Aur	9177	914	125	9000	0.984	
V1647 Sgr	9361	535	125	8750	0.948	
VV Pyx	9751	782	125	9500	1.00	
Group IV						
χ ² Hya	12160	1370	250	11500	0.945	
Group III						
		T ₂	Err	Err	T ₁	
			SD	Vis		
WX Cep	9087	1092	125	8375	1.08	
V1031 Ori	8906	419	100	7750	1.07	
AY Cam	7590	318	150	7200	1.02	

NOTE—^a The T₂/T₁ is from TAG; ^b 1T: one temperature model fit

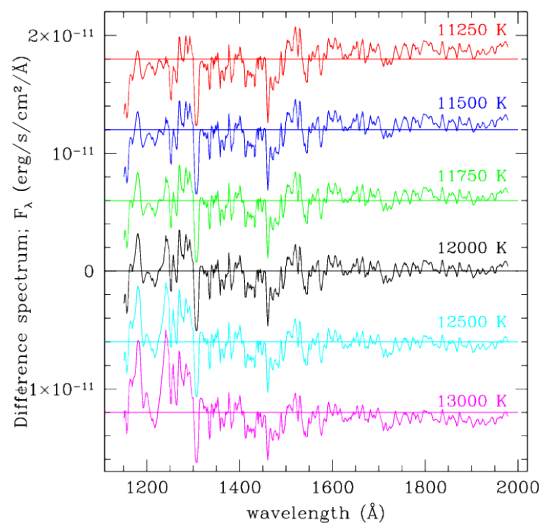


Figure 2. V451 Oph: The difference between the composite model and the spectrum. The differences from models of six T_1 temperatures (indicated in the figure) are shown from top to bottom. An arbitrary constant has been added to the difference spectra so that they do not overlap. (T_2 fixed at 9800 K.) The best fit is indicated with a black line. The changes as a function of model temperature are clear in the comparison. The coolest model (top) is too low in flux for the shorter wavelengths as compared with the (normalized) longer wavelengths. Conversely, for a hotter model (bottom) the model fluxes are larger than the spectrum for wavelengths shorter than 1300 Å. In this temperature range, the poor agreement in the Ly α region near 1200 Å is particularly marked for the hottest model.

5.1. V478 Cyg

The temperature for V478 Cyg has one of the largest uncertainties in this study for two reasons. First, it is one of the weakest exposures. In addition to that the $E(B-V)$ is somewhat uncertain. The $E(B-V)$ in TAG is 0.85, taken from Popper and Etzel (1981). As they discuss, the B-V measurement of the system (Popper and Dumont 1977) was done with two telescopes (Palomar and Kitt Peak). The larger diaphragm at Palomar included an additional star. This star is 4.26 mag fainter than V478 Cyg, hence would have only a very small effect on the color, most likely making it slightly redder. Since photometry of the system is typically made differentially, measurements of B-V are scarce. We were not able to achieve a definitive fit, and omit V478 Cyg from further consideration.

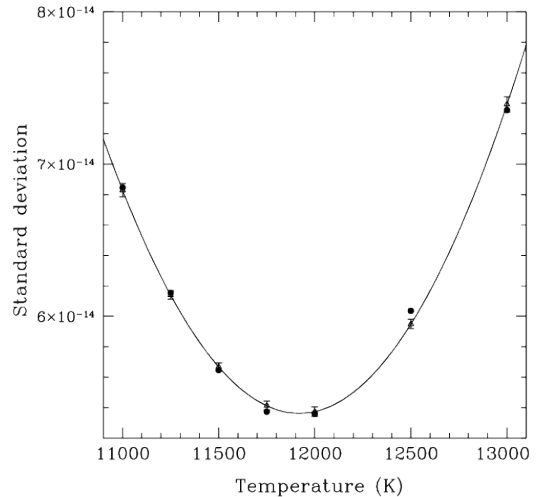


Figure 3. V451 Oph: The temperature determination: the standard deviation as a function of temperature of the primary. The temperature of the secondary was fixed at 11000 K; dots: the standard deviation from the spectrum-model comparison; triangles: the parabola fit.

5.2. AH Cep

The *IUE* spectrum of AH Cep is saturated for half the wavelength region. For this reason, the standard temperature fitting is unreliable. AH Cep is omitted from Mass-Temperature fitting.

5.3. U Oph

Although the exposure of U Oph is reasonably good, the spectrum is saturated in several important wavelength regions. For this reason, it is omitted from temperature discussions.

5.4. QX Car

The temperatures of the two components are similar (Group I), but the masses are clearly not identical (TAG). We have investigated both 1T and 2T fits. The temperature from the 2T fit is 23430 K, with an estimated visual uncertainty of 1000 K.

5.5. V578 Mon

Because the spectrum rises monotonically toward short wavelengths, the temperature and reddening are degenerate, therefore the temperature from the *IUE* spectrum is not definitive, and is not used in subsequent temperature discussions. Subsequent to TAG, a small adjustment was made to the ratio of radii (Garcia, et al. 2013), resulting in a difference of the normalization factor $(R_2/R_1)^2$ of 2%, which has no effect on T_1 .

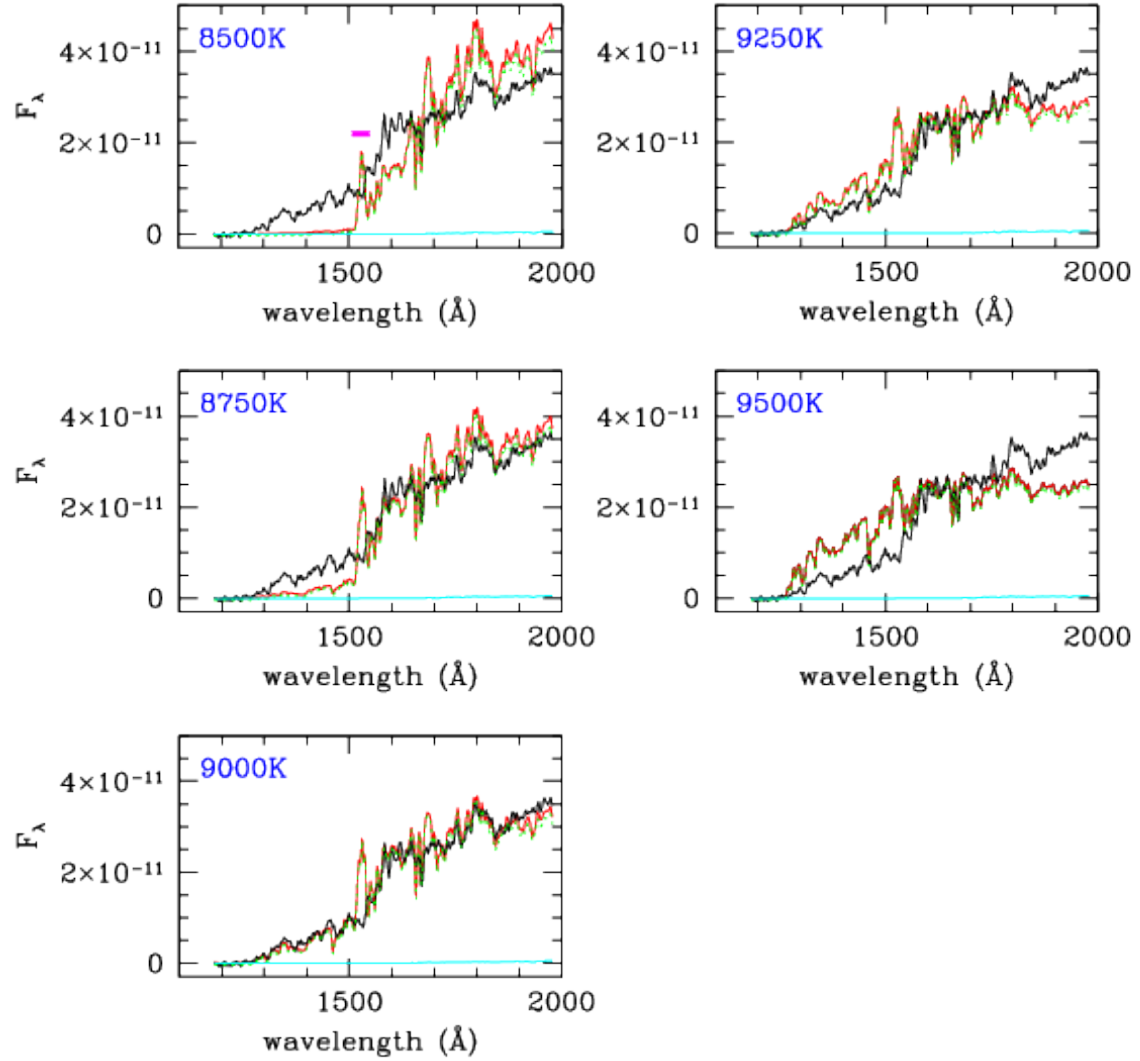


Figure 4. YZ Cas: Comparison of *IUE* spectrum and models. Lines are the same as in Fig 1. The magenta line above the spectrum in the upper left at 1550 \AA indicates that this feature was not included in the fit. Best fit is for $T_1 = 9000$ K.

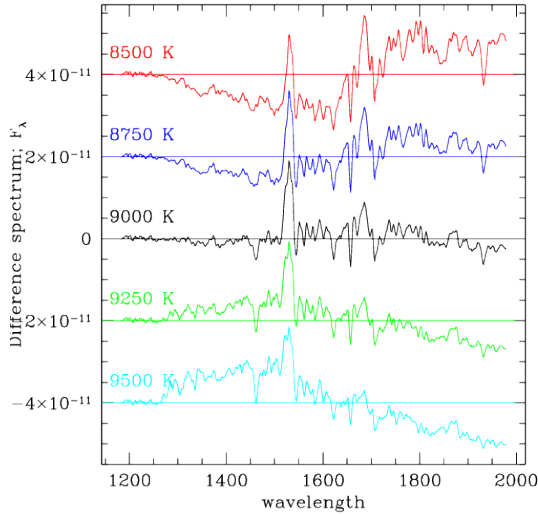


Figure 5. YZ Cas: The difference between the model and the *IUE* spectrum. The differences from models of five temperatures is shown from top to bottom with increasing model temperature. The best fit is indicated with a black line.

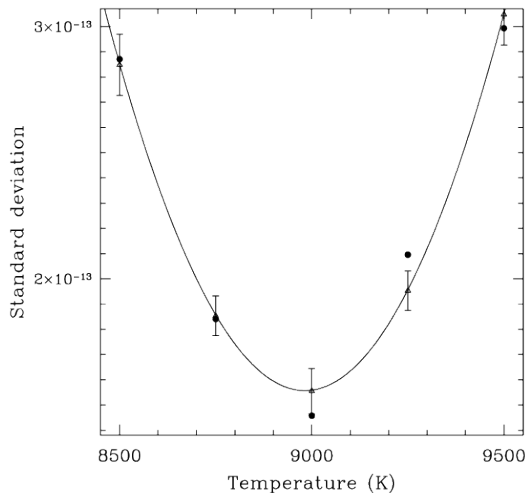


Figure 6. YZ Cas: The temperature determination: the standard deviation as a function of temperature of the primary. The temperature of the secondary was fixed at 7250 K; dots: the standard deviation from the spectrum-model fit; triangles: the parabola fit

5.6. V539 Ara

The *IUE* observation occurred just inside the start of primary eclipse. However, V539 Ara is a Group II system, with the secondary significantly less luminous than the primary in the ultraviolet. The decrease in flux in the primary of approximately 5% will have minimal effect on the spectral fitting. (Fig. 1 illustrates a similar system.)

5.7. Group III: WX Cep, and V1031 Ori, and AY Cam

For the three stars in this group the hotter star is actually the secondary which is less luminous, and smaller, so the more massive star is less dominant in the ultraviolet. For this reason it is more difficult to disentangle the composite spectrum, and the temperature of the hotter star is less well determined. We include estimates of the temperatures in Tables 4 and 6 but they are omitted from the Mass-Temperature relation determination.

5.8. Group IV: χ^2 Hya

In this system, the primary is significantly evolved beyond the main sequence (Clausen and Nordstrom 1978). For this reason, it is not used in the main sequence Mass-Temperature relation determination.

6. HOT STARS

One of the aims of this project was to explore the upper range of temperature where *IUE* spectra provide definitive temperatures. The hottest stars in the sample (V478 Cyg, AH Cep, and V578 Mon) did not produce well determined temperature (Section 5). U Oph also was unsatisfactory because of the overexposed spectrum

Ribas et al. (2000) have determined the temperatures from photometry, compared with Kurucz atmospheres. In order to check the upper temperature limit for which the *IUE* spectra are accurate, the temperature determinations of the two hottest stars in the *IUE* DEB sample are compared with the Ribas et al. temperatures in Table 5. The temperatures of the two hottest stars agree within the errors.

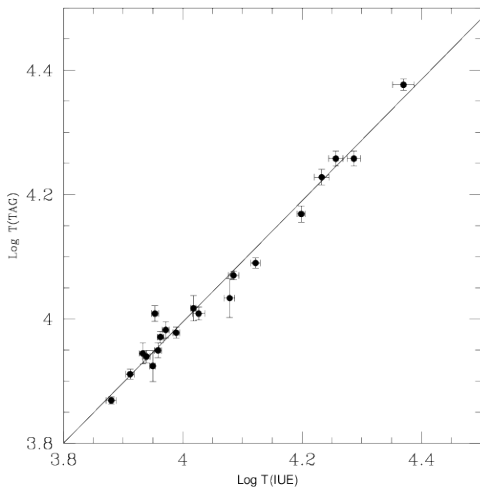
7. DISCUSSION

7.1. Binary Parameter Summary

Parameters for the DEB systems are summarized in Table 6. Each system has two rows, one for the primary and one for the secondary. The first entry is the name of the system (line 1) and the HD or BD number (line 2). The next columns are the spectra type, the mass and its error in M_{\odot} , the temperature and its error in K, the radius and its error in R_{\odot} , the E(B-V) and its error (where known) in mag, the temperature and error from

Table 5. Temperatures of Early B Stars

Spect		T	T
Type		Table 4	Ribas et al. (2000)
		(K)	(K)
QX Car	B2 V	23428 ± 1000	24831 ± 520
CV Vel	B2.5 V	18045 ± 500	17947 ± 500


Figure 7. The temperatures from the *IUE* spectral fit $\text{Log } T(\text{IUE})$ versus the temperatures from TAG $\text{Log } T(\text{TAG})$. Both temperatures are in K.

this study (Table 4), and the log luminosity in solar units (Section 7.7). The mass, spectral type, radius, temperature, and $E(B-V)$ are from TAG. $E(B-V)$ for WX Cep is from Graczyk et al (2019).

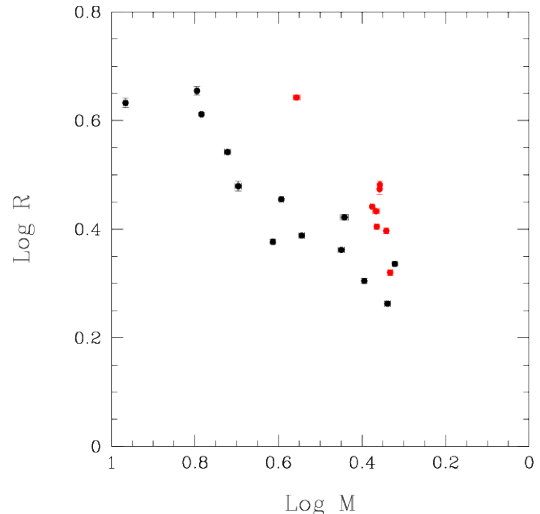
7.2. Comparison between T_{IUE} and T_{TAG}

The comparison between the log of the IUE temperatures derived here from spectral fits and the log of the temperatures from TAG is shown in Fig. 7. In general they are similar within the errors, with an insignificant offset. The line shows the fit from the least squares bisector (unweighted), as recommended by Isobe, et al. (1990):

$$\log T(\text{TAG}) = 0.104 \pm 0.114 + (0.973 + 0.020) \times \log T(\text{IUE}) \quad (\text{Eqn 1})$$

7.3. The M - R Relation: Evolution

The Log Mass–Log Radius relation from TAG data is shown in Fig. 8. Stars with radii larger than the main


Figure 8. Log Radius vs Log Mass relation from the TAG sample. Main sequence stars are in black; other stars are in red. The group of other stars includes χ^2 Hya, Group III stars, and Am stars (see text). Masses are in M_{\odot} ; radii are in R_{\odot}

sequence minimum indicates evolution beyond the Zero Age Main Sequence, which is a major source of scatter in the Mass–Temperature relation. The stars marked in red in Fig. 8 are from several groups identified in this study. They include χ^2 Hya, which is known to be evolved. Group III stars are also evolved. In this case it is the temperature of the secondary which we determine. The primary is clearly evolved in Group III systems, but the secondary may also be. In fact, for all three stars (WX Cep, V1031 Ori and AY Cam), the radius is larger than the radii for the main sequence. The 5 stars with an Am (metallic) primary (β Aur, YZ Cas, V624 Her, GZ CMa, and EE Peg) are discussed in the next section. All these stars shown in red sit above the main sequence relation in Fig. 8, and account for most of the spread in the Log M –Log R relation. This is discussed further in the next section.

7.4. Metallicity

Five stars in the DEB sample have a metallic Am primary (β Aur, YZ Cas, V624 Her, GZ CMa, and EE Peg). In the previous section and Fig. 8, it was shown that they have larger radii (for a given mass) than normal A stars. In this case, they are not necessarily evolved, simply showing the effects of a metal-rich atmosphere. In the mass–temperature relation in the next section, they typically have cooler temperatures than normal A stars coupled with their larger radii. Again, this is explained by a metal-rich atmosphere. In addition, the BOSZ models used here assume solar abundances, and

Table 6. Parameters for the DEB Sample

System	SpecType	Mass	\pm	T	\pm	Radius	\pm	E(B-V)	\pm	T	\pm	Log Lum
		(M_{\odot})	(M_{\odot})	(K)	(K)	(R_{\odot})	(R_{\odot})	(mag)	(mag)	(K)	(K)	(L_{\odot})
				TAG	TAG					IUE	IUE	
V478 Cyg	O9.5V	16.62	0.33	30479	1000	7.426	0.072	0.85
HD 193611	O9.5V	16.27	0.33	30549	1000	7.426	0.072
AH Cep	B0.5Vn	15.26	0.35	29900	1000	6.346	0.071	0.58	0.08
HD 216014	B0.5Vn	13.44	0.25	28600	1000	5.836	0.085
V578 Mon	B1V	14.50	0.12	30000	740	5.149	0.091	0.455	0.029
HD 259135	B2V	10.262	0.084	26400	600	4.21	0.10
QX Car	B2V	9.25	0.12	23800	500	4.291	0.091	0.049	...	23428	1000	3.6701
HD 86118	B2V	8.46	0.12	22600	500	4.053	0.091
V539 Ara	B3V	6.24	0.066	18100	500	4.516	0.084	0.071	...	19248	500	3.3828
HD 161783	B4V	5.314	0.06	17100	500	3.428	0.083
CV Vel	B2.5V	6.086	0.044	18100	500	4.089	0.036	0.035	...	18045	500	3.1535
HD 77464	B2.5V	5.982	0.035	17900	500	3.950	0.036
U Oph	B5V	5.273	0.091	16440	250	3.484	0.021	0.226	0.007
HD 156247	B6V	4.739	0.072	15590	250	3.110	0.034
V760 Sco	B4V	4.969	0.09	16900	500	3.015	0.066	0.33	...	17092	500	2.8112
HD 147683	B4V	4.609	0.073	16300	500	2.641	0.066
GG Lup	B7V	4.106	0.044	14750	450	2.380	0.025	0.027	...	15793	250	2.3995
HD 135876	B9V	2.504	0.023	11000	600	1.726	0.019
ζ Phe	B6V	3.921	0.045	14400	800	2.852	0.015	0	...	14483	250	2.5539
HD 6882	B8V	2.545	0.026	12000	600	1.854	0.011
χ^2 Hya	B8V	3.605	0.078	11750	190	4.390	0.039	0.016	...	12160	250	2.4619
HD 96314	B8V	2.632	0.049	11100	230	2.159	0.030
IQ Per	B8V	3.504	0.054	12300	230	2.445	0.024	0.14	0.01	13241	250	2.1479
HD 24909	A6V	1.730	0.025	7700	140	1.499	0.016
PV Cas	B9.5V	2.816	0.05	10200	250	2.301	0.020	0.217	...	10632	250	1.7687
HD 240208	B9.5V	2.757	0.054	10190	250	2.257	0.019
V451 Oph	B9V	2.769	0.062	10800	800	2.642	0.031	0.158	...	11980	250	1.9555
HD 170470	A0V	2.351	0.052	9800	500	2.029	0.028
WX Cep	A5V	2.533	0.05	8150	250	3.996	0.03	0.19	0.03
HD 213631	A2V	2.324	0.045	8900	250	2.712	0.023	9087	125	...
TZ Men	A0V	2.482	0.025	10400	500	2.017	0.02	0	...	10418	100	1.6741
HD 39780	A8V	1.500	0.010	7200	300	1.433	0.014
V1031 Ori	A6V	2.468	0.018	7850	500	4.323	0.034	0.034
HD 38735	A3V	2.281	0.016	8400	500	2.978	0.064	8906	100	...
β Aur	A1m	2.375	0.027	9350	200	2.765	0.018	0	...	9177	125	...
HD 40183	A1m	2.304	0.030	9200	200	2.571	0.018
YZ Cas	A1m	2.317	0.020	10200	300	2.539	0.026	0.07	...	8982	125	1.7423
HD 4161	F2V	1.352	0.009	7200	300	1.350	0.014
V624 Her	A3m	2.277	0.014	8150	150	3.031	0.051	0.05	0.01	8160	125	1.5924
HD 161321	A7m:	1.876	0.013	7950	150	2.210	0.034
GZ CMa	A3m	2.199	0.017	8800	350	2.494	0.031	0.07	0.03	8566	125	1.4951
HD 56429	A4V:	2.006	0.012	8500	350	2.132	0.037
V1647 Sgr	A1V	2.184	0.037	9600	300	1.832	0.018	0.04	...	9361	125	1.4346
HD 163708	A1V	1.967	0.033	9100	300	1.667	0.017
EE Peg	A3m	2.151	0.024	8700	200	2.090	0.025	0	...	8687	125	1.2871
HD 206155	F5V	1.332	0.011	6450	300	1.312	0.013
VV Pyx	A1V	2.097	0.022	9500	200	2.168	0.02	0.022	...	9751	125	1.7809
HD 71581	A1V	2.095	0.019	9500	200	2.168	0.02
AY Cam	A0V	1.905	0.04	7250	100	2.772	0.02	0.06
BD+77 328	F0V	1.707	0.036	7395	100	2.026	0.017	7590	150	...

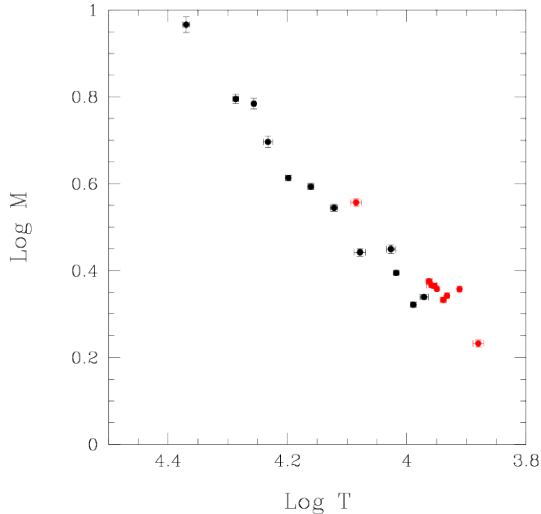


Figure 9. The Mass -Temperature relation. Main sequence stars: black; others: red. Others include χ^2 Hya, Group III stars, and Am stars. Masses are in M_{\odot} ; temperatures are in K.

hence are not appropriate for Am stars. For this reason these stars are omitted from the determination of the Mass-Temperature relation.

7.5. The M-T Relation

The relation between mass and temperature is shown in Fig. 9. (The errors in the temperatures are from the visual inspection.) The systems plotted in black are used to determine the relation (omitting stars showing evolution and chemically peculiar stars plotted in red).

For this limited temperature (23000 to 8000K) and mass range, we have assumed a linear relation between $\log M$ and $\log T$. The relation from bisector least squares is:

$$\log M/M_{\odot} = -5.90 \pm 0.27 + (1.56 \pm 0.07) \times \log T \quad (\text{Eqn 2})$$

The RMS of the residuals from the fit of the $\log M/M_{\odot}$ is 0.037.

This mass-temperature relation is directly determined. However, there are several factors which contribute to the width of the relation. Different rotation velocities and different abundances will result in a spread in temperatures between stars. In addition during their main sequence lifetimes, stars cool, resulting in a range of temperatures. As an example, the evolutionary tracks from Ekström, et al. (2012) span approximately 0.1 dex in $\log T$ during the main sequence. This corresponds to an uncertainty of approximately 0.08 dex in $\log M$ or about 18%. The scatter about the mean relation (± 0.04 dex in $\log M$) due to evolution within the main sequence is about the same as the RMS around equation

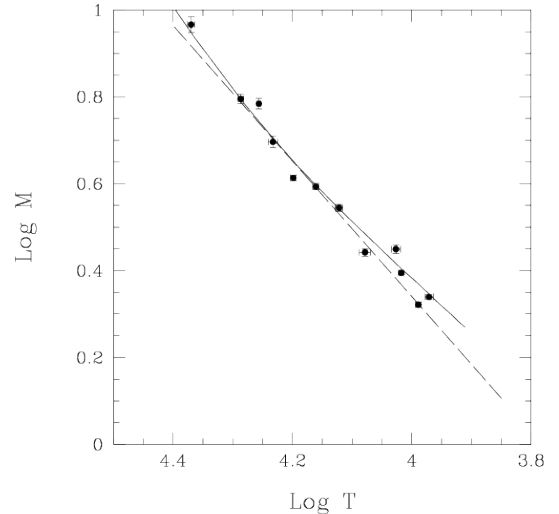


Figure 10. The Mass -temperature relation. Main sequence stars: black points; dashed line: fit to points; solid line: Harmanec relation.

2. That is, the age spread accounts for at least a large part of the RMS scatter.

In certain cases, this age-related uncertainty is lower. For instance, a secondary which is the companion of a more massive star must be comparatively young. The hot companion of a Cepheid is an example which must be close to the zero age main sequence (ZAMS). That is, it will be on the hotter edge of the M-T relation with a smaller uncertainty than a random main sequence star.

7.6. Comparisons Against Other M-T Relations

The linear fit to the main sequence points (black points in Fig. 9) is shown in Fig. 10 in the dashed line. Harmanec (1988) used the sample of DEBs available at that time to derive a Mass-Temperature relation over the full length of the main sequence. The solid line shows the relation from Harmanec (1988). The Harmanec relation is curved since it describes a much larger temperature range. However the agreement is essentially good in this temperature range.

7.7. The Luminosity-Temperature Relation

For completeness we provide the Log Temperature – Log Luminosity relation in Fig. 11. Luminosities are derived from TAG values scaled by $(T_{IUE}/T_{TAG})^4$. The stars shown omit systems showing evolution (χ^2 Hya, WX Cep, V1031, and AY Cam), as well as Am stars.

8. CONCLUSIONS

This study combines masses for DEBs with temperatures determined from ultraviolet IUE spectra and BOSZ model atmospheres. For this important group on

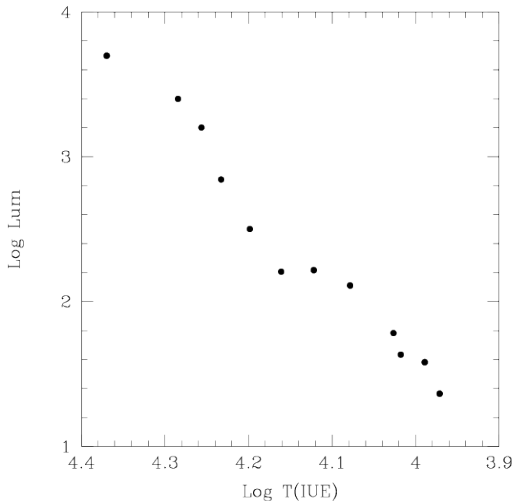


Figure 11. The Log Temperature–log Luminosity relation for main sequence stars showing no evolution or chemical peculiarities (see text). Luminosity is in solar units; the temperature is determined from the IUE spectral fits.

which the calibration of masses on the main sequence rests, a direct Mass-Temperature relation is determined for B and early A stars. The mass-radius plot (Fig 8) shows that some of the sample is evolved beyond the main sequence. These stars as well as chemically peculiar Am stars have been removed from the calibration sample. The Mass-Temperature relation is probably still somewhat broadened by variation in evolution and abundance, however Fig. 9 demonstrates that the scatter is relatively small (RMS of the $\log M/M_{\odot}$ is 0.037). The comparison between the IUE temperatures and those in TAG from spectral types is good. Furthermore, the Mass-Temperature relation is very similar to that derived by Harmanec (1988).

9. ACKNOWLEDGMENTS

The authors would like to thank Dr. Hans Moritz Günther for his insightful comments and assistance regarding our temperature fitting. We thank the referee for comments that improved the content of the paper as well as the presentation. It is a pleasure to thank

Dr. Richard Gray for comments on chemically peculiar stars. M.G.F would like to thank Dr. Matt Ashby and Dr. Jonathan McDowell for their invaluable comments and guidance during the SAO REU program. The SAO REU program is funded in part by the National Science Foundation REU and Department of Defense ASSURE programs under NSF Grant no. AST-2050813, and by the Smithsonian Institution. Support was provided to N.R.E. by HST Grant GO-15861.001-A and by the Chandra X-ray Center NASA Contract NAS8-03060. This research is based on observations made with the *IUE* satellite, obtained from the MAST data archive at the Space Telescope Science Institute, which is operated by the Association of Universities for Research in Astronomy, Inc., under NASA contract NAS 5–26555. This research has made use of the SIMBAD database, operated at CDS, Strasbourg, France.

10. APPENDIX A: EARLY B STARS

In order to confirm the temperature sensitivity of the IUE spectra of the hotter stars in the DEB sample we examined stars from the *IUE* Spectral Atlas (Wu, et al. 1983). The *IUE* Atlas project observed samples of the full range of the Morgan-Keenan (MK) spectral system in low dispersion in both the short and long wavelength regions, primarily using stars defining the MK classes. Table 7 lists the spectra selected for this test for spectral classes B1 V, B3 V, and B5 V. Columns provide the spectral type, the HD number, V, E(B-V), the *IUE* spectrum number, the exposure level, alternate designations, MK for stars which define MK classes, and the temperature, and the temperature uncertainty from the SD comparisons, and from visual comparisons. The maximum exposure is in instrumental Data Numbers (DN), where an optimal exposure is near 200 DN. The spectra were fitted to BOSZ models (1T fit). The resulting temperatures are listed in Table 7. The final three columns list temperatures for these classes for 3 widely used calibrations of temperatures for MK classes: Drilling and Landolt in *Astrophysical Quantities* (2000), Harmanec (1988) and Pecaut and Mamajek (2013). The agreement is reasonable, given that MK classes have some width in temperature. Lyubimkov et al. (2002) derive $T=22500 \pm 600$ K for HD31726, which is close to the *IUE* result

REFERENCES

- Andersen, J. 1983, *A&A*, 118, 255
 Andersen, J., Clausen, J. V., Nordstroem, B., et al. 1983, *A&A*, 121, 271
 Andersen, J., Clausen, J. V., & Gimenez, A. 1993, *A&A*, 277, 439
 Andersen, J., Clausen, J. V., Nordstrom, B., et al. 1985, *A&A*, 151, 329
 Andersen, J., Clausen, J. V., & Nordstrom, B. 1984, *A&A*, 134, 147

Table 7. *IUE* Observations of MK Standard Stars

Spectral Type	HD	V	E(B-V)	Spectrum	Exp Max	ID	T	±	±	AQ	Harm	PM	
		(mag)	(mag)		(DN)		(K)	(K)	SD	Vis	(K)	(K)	(K)
B1 V	31726	6.15	0.05	SWP8165	230		22471.0	908	500	24540	26180	26000	
B3 V	190993	5.06	0.02	SWP9961	200	17 Vul MK	18025.1	401	500	19000	19050	17000	
B5 V	34759	5.22	0.02	SWP15537	190	ρ Aur MK	16373.3	378	375	15200	15490	15700	

AQ: Drilling, and Landolt (2000)

Harm: Harmanec (1988)

PM: Pecaut and Mamajek (2013)

- Andersen, J., Clausen, J. V., & Nordstrom, B. 1987, *A&A*, 175, 60
- Andersen, J., Clausen, J. V., & Nordstrom, B. 1990, *A&A*, 228, 365
- Andersen, J. & Gimenez, A. 1985, *A&A*, 145, 206
- Andersen, J. 1991, *A&ARv*, 3, 91.
- Barenbaum, M. J. & Etzel, P. B. 1995, *AJ*, 109, 2680
- Bohlin R. C. and Bianchi, L 2017, *AJ*, 155, 162
- Bohlin, R. C., Meszaros, S., Fleming, S. W., Gordon, K. D., Koekemoer, A. M. and Kovacs, J. 2017, *AJ*, 153, 23
- Cardelli, Clayton, and Mathis 1989, *ApJ* 345, 245
- Clausen, J. V. 1996, *A&A*, 308, 151
- Clausen, J. V., Gimenez, A., & Scarfe, C. 1986, *A&A*, 167, 287
- Clausen, J. V. and Nordstrom, B. 1978, *A&A*, 67, 15
- Drilling, J. S., and Landolt, A. U. in Cox, A. N. 2000, *Astrophysical Quantities*, Springer: London, 388
- Ekström, S., Georgy, C. and Eggenberger, P. et al. 2012, *A&A*, 537, A146
- Garcia, E. V., Stassun, K. G., and Torres, G. 2013, *ApJ*, 769, 114
- Graczyk D., Pietrzynski G., Gieren W. et al. 2019, *ApJ*, 872, 85
- Harmanec, P. 1988, *Bull. Astron. Inst. Czechosl*, 39, 329
- Harris, A. W. and Sonneborn, G. 1987, in *Exploring the Universe with the IUE Satellite*, ed. Y. Kondo, et al. (Reidel Publishing Company, Dordrecht, Holland), 729
- Hensberge, H., Pavlovski, K., and Verschueren, W. 2000 *A&A*, 358, 553
- Holmgren, D. E., Hill, G., and Fisher, W. 1990, *A&A*, 236, 409
- Isobe, T., Feigelson, E. D., Akritas, M. G., and Babu, G. J. 1990, *ApJ*, 364, 104
- Lacy, C. H. and Popper, D. M. 1984, *ApJ*, 281, 268
- Lyubimkov, L. S., Rachkovskaya, T. M., Rostopchin, S. I., and Lambert, D. L. 2002, *MNRAS*, 333, 9
- Nichols, J. S. and Linsky, J. L. 1996, *AJ*, 111, 517
- Pavlovski, K., Southworth, J., Kolbas, V., et al. 2014, *MNRAS*, 438, 590
- Pecaut, M. J. and Mamajek, E. E. 2013, *ApJS*, 208, 9
- Popper, D. M. 1987, *AJ*, 93, 672
- Popper, D. M. and Dumont, P. J. 1977, *AJ*, 82, 216
- Popper, D. M. and Etzel, P. B. 1981, *AJ*, 86, 102
- Popper, D. M. 1984, *AJ*, 89, 1057
- Popper, D. M., Andersen, J., Clausen, J. V., et al. 1985, *AJ*, 90, 1324
- Ribas, I., Jordi, C., Torra, J., and Gimenez, A. 2000, *MNRAS*, 313, 99
- Southworth, J., Bruntt, H., & Buzasi, D. L. 2007, *A&A*, 467, 1215
- Torres, G., Andersen, J., and Gimenez, A. 2010, *A&ARv*, 18, 67 (TAG)
- Vaz, L. P. R., Andersen, J., & Claret, A. 2007, *A&A*, 469, 285
- Williamon, R. M., Sowell, J. R., & Van Hamme, W. 2004, *AJ*, 128, 1319
- Wolf, M., Kučáková, H., Kolasa, M., et al. 2006, *A&A*, 456, 1077.
- Wu, C.-C., Ake, T. B., Boggess, A. et al. 1983, *IUE Newsletter #22*
- Yakut, K., Aerts, C., & Morel, T. 2007, *A&A*, 467, 647